

RESEARCH ARTICLE

Enhanced oil recovery mechanism and recovery performance of micro-gel particle suspensions by microfluidic experiments

Wenhai Lei¹ | Tong Liu¹ | Chiyu Xie² | Haien Yang³ | Tianjiang Wu³ | Moran Wang¹ ¹Department of Engineering Mechanics, Tsinghua University, Beijing, China²Department of Petroleum and Geosystems Engineering, The University of Texas, Austin, TX, USA³Changqing Oilfield, PetroChina, Xi'an, China**Correspondence**

Moran Wang, Department of Engineering Mechanics, Tsinghua University, Beijing 100084, China.

Email: mrwang@tsinghua.edu.cn

Funding information

NSF, Grant/Award Number: U1837602 and 91634107; National Science and Technology Major Project on Oil and Gas, Grant/Award Number: 2017ZX05013001

Abstract

Micro-gel particle suspensions (MGPS) have been proposed for enhanced oil recovery (EOR) in reservoirs with harsh conditions in recent years, yet the mechanisms are still not clear because of the complex property of MGPS and the complex geometry of rocks. In this paper, the micro-gel particle-based flooding has been studied by our microfluidic experiments on both bi-permeability micromodels and reservoir-on-a-chip. A method for reservoir-on-a-chip design has been proposed based on QSGS (quartet structure generation set) to ensure that the flow geometry on chip owns the most important statistical features of real rock microstructures. In the micromodel experiments with heterogeneous microstructures, even if the MGPS has the same macroscopic rheology as the hydrolyzed polyacrylamides (HPAM) solution for flooding, MGPS may lead to significant fluctuations of pressure field caused by the nonuniform concentration distribution of particles. In the reservoir-on-a-chip experiments, clustered oil trapped in the swept pores can be recovered by MGPS because of pressure fluctuation, which hardly happens in the HPAM flooding. Compared with the water flooding, the HPAM solution flooding leads to approximately 17% incremental oil recovery, while the MGPS results in approximately 49.8% incremental oil recovery in the laboratory.

KEYWORDS

enhanced oil recovery, flooding recovery, microfluidics, micro-gel particle, reservoir-on-a-chip

1 | INTRODUCTION

Oil and gas still supply most of the world's energy, and extraction of the remaining trapped oil is significant to meet the demand of near-future energy.^{1,2} Due to the reservoir heterogeneity and high oil viscosity, it is reported that the normal water flooding can only produce about 30% of the original oil generally.³ The nonuniform fluid displacements in porous media are commonly observed in water flooding, so that the water cut will continue to rise until it reaches a high value.⁴

Various enhanced oil recovery (EOR) techniques have been applied to overcome this challenging problem and significantly increase hydrocarbon recovery, including polymer flooding,⁵⁻⁷ foam displacement,^{8,9} gas injection,¹⁰ and so on. Among these techniques, the polymer flooding is considered as one of the most promising technologies. Water-soluble polymers such as xanthan gums and hydrolyzed polyacrylamides (HPAM) have been successfully implemented,⁵⁻⁷ and the oil production can be improved by increasing the sweep volume of reservoir and the displacement efficiency of oil.

This is an open access article under the terms of the Creative Commons Attribution License, which permits use, distribution and reproduction in any medium, provided the original work is properly cited.

© 2019 The Authors. *Energy Science & Engineering* published by the Society of Chemical Industry and John Wiley & Sons Ltd.

The high viscous property provides a good way for mobility control, yet the injection capacity reduction, shear degradation (in high temperature and high salinity), and dilution effect limit their applications. In recent years, the particle-type polymers, such as preformed particle gel (PPG),^{4,11} colloidal dispersed gels (CDG),^{12,13} polymer microsphere,^{14,15} have been developed as a smart agent for sweep improvement and profile modification. In our study, we classify the particles at micron and nanometer size as the micro-gel particles which can transport easier in the deep formation. The micro-gel particle is a network of aggregated colloidal particles with soft solid-like mechanical properties.^{16,17} The micro-gel particle suspension is a kind of viscoelastic fluid, and the micro-gel particles are cross-linked as a porous interconnected network structure at microscale.¹⁸ The fact is that micro-gel particle suspension is not always effective for all kinds of oilfields in practice^{19,20} due to unclearness of its transport mechanism. Understanding the transport mechanism of micro-gel particle suspension in porous media is crucial for gel treatments during enhanced oil recovery.

Numerous studies have been conducted to evaluate transport of different kinds of micro-gel particle suspension in porous media at core scale. Smith et al²¹ compared micro-gel particle suspension with water-solute polymer in core-flooding experiments. The micro-gel particle suspension showed a similar injectivity as the water-solute polymer but a stronger impact on permeability reduction of rocks. Almohsin et al²⁰ conducted core-flooding experiments which showed that the flow resistance increased with the micro-gel particle concentration. Imqam et al⁴ studied the factors for the micro-gel particle transport behaviors and found that the micro-gel particle injection was more sensitive to the micro-gel particle strength than the micro-gel particle size and that the micro-gel particles could go deep into sandstones. Sand-packed experiments^{13,14,22} were conducted and showed that the micro-gel particles easily entered the in-depth formations and effectively plugged high-permeability channels to improve effects of profile control. Up to now, the most popular explanation of micro-gel particle transport mechanisms is blocking the fluid channeling paths and diverting the displacing fluid from the higher-permeability layer to the lower-permeability layer (so-called diversion effect), which causes the higher pressure to push the micro-gel particle to deform and pass through the pore throats. However, those core scale experiments hardly provided any direct evidence of micro-gel particle suspension transport behavior because of difficulties of visualizing dynamic multiphase flows in cores.

With developments of microchips, microfluidics or micromodel provides a powerful tool to study pore-scale flow and EOR mechanism.^{23,24} Compared with the core-flooding experiments, microfluidics has significant advantages in visualization, controllability, and repeatability. Using this microfluidic technology, a few studies have been conducted on

gel particle transport process. Bai et al¹¹ used etched glass micromodels with structured geometries to study transport process of PPG particles through throat channels. They reported the PPG propagation patterns of behavior and showed that the particle transport behaviors depended on the gel strength, threshold pressure, and throat structure. Yao et al¹⁵ conducted experiments using packed quartz sands in between two transparent plates to observe micro-gel particle transport behaviors, such as capture-plugging, superposition-plugging, and bridge-plugging, all of which actually produced resistance to water flow. Since the sand-packed model is far from representing real rock features including pore distribution and formation, a 3D-printed milli-fluidic device with structured pore-throat geometries was fabricated by O'Connell et al.²⁵ They found that the cooperative size sorting mechanism of millimeter hydro-gel particles caused the particles to ultimately sort themselves by size through the pore space when particle size was comparable with channel diameter. As reported, the visual experiments on microchips have provided a powerful tool to study the particle transport behavior, which strongly depends on the particle properties and the pore geometries. The challenges for further studies come from how to characterize the particle properties correctly¹⁷ and how to make the micromodel geometries closer to the real rocks.

Even though the flow in a 2D microchip is not exactly the same as that in 3D rocks, some appropriate features of real rocks can still be represented by microfluidic systems fabricated with different geometries.²⁶ More importantly, visualized microfluidics experimental results can be compared with numerical simulation results directly,^{27,28} which could make up disadvantages of microfluidics in 3D geometry. Based on number of pores, we can divide the microfluidic experiments roughly into three types: microchannel chip^{25,29} (one to several pores); micromodel^{9,30} (dozens to hundreds of pores); and reservoir-on-a-chip³¹⁻³³ (thousands of pores). Microchannel chips and micromodels are generally artificial geometries to represent special pore features. For actual geological features, some chips with complex geometries were designed based on scanned images of a sliced real rock³⁴ or a pore-network model.³¹ Such image-based geometries made the chips appear more realistic, yet the similarity of pore connectivity was not seriously proved with real rocks, which actually influences significantly the permeability, phase distribution, and interaction of fluids.

In this paper, we present our microfluidic experimental framework to study the micro-gel particle-based EOR mechanisms. We use structured bi-permeability geometry to study the transport mechanism of micro-gel particle suspension in heterogeneous porous media. Subsequently, we propose a strategy to generate equivalent geometries based on statistical information of real core/reservoir structures by the QSGS method^{35,36} on a chip, namely so-called reservoir-on-a-chip. The reservoir-on-a-chip experiments were conducted

to evaluate the displacement performance of micro-gel particle suspension. The experimental results can improve understandings of transport behaviors and EOR mechanism of micro-gel particle suspension in cores or reservoirs.

2 | EXPERIMENTAL METHODS

The experimental elements and methods are introduced as follows.

2.1 | Fluids preparation

Decane (molecular weight = 142.28 g/mol, viscosity = 0.80 mPa·s, density = 0.73 g/mL) was selected as the oleic phase in our experiments, and it was transparent to be dyed by Nile red fluorescence with 100 ppm concentration. Deionized (DI) water (viscosity = 0.91 mPa·s, density = 0.997 g/mL, resistivity = 18 M Ω ·cm) was used as water phase in water flooding or solvent. Hydrolyzed polyacrylamide (HPAM, molecular weight = 24×10^6 g/mol) was obtained from Sangon Biotechnology.

Inverse micro-emulsion polymerization techniques were used to make highly concentrated micro-gel particle suspension (original suspension, about 20 wt% particle content), and micro-gel particles with fluorescence were realized by Technical Institute of Physics and Chemistry, Chinese Academy of Sciences. The particle size distribution of micro-gel particle suspension was measured by Mastersizer 3000 particle size analyzer (Malvern) instrument. The particle size distribution and morphology of the micro-gel particles are shown in Figure 1. The mean particle size is 7.64 μ m, and the main particle size range is 3.55–24.1 μ m.

A cryo-scanning electron microscope (FEI Helios NanoLab G3UC) was used to study the structural features of the micro-gel particles. Cryo-scanning electron micrographs of the micro-gel particles at various magnifications are presented in Figure 2. The particles appeared to be roughly spherical with an average diameter of 5 μ m, and under higher magnification, the internal structure of polymer network can be observed (Figure 2B).

2.2 | Rheology property

The experimental temperature was controlled at a constant 20°C. A cone-plate measuring system with a diameter of 60 mm was used in this measurement. In order to make the HPAM solution and the micro-gel particle suspension with the similar macroscopic rheology property, the HPAM solution concentration was set as 200 mg/L and the highly concentrated micro-gel particle suspension was diluted at 3 vol% by DI water. The shear stress and the apparent viscosity of micro-gel particle

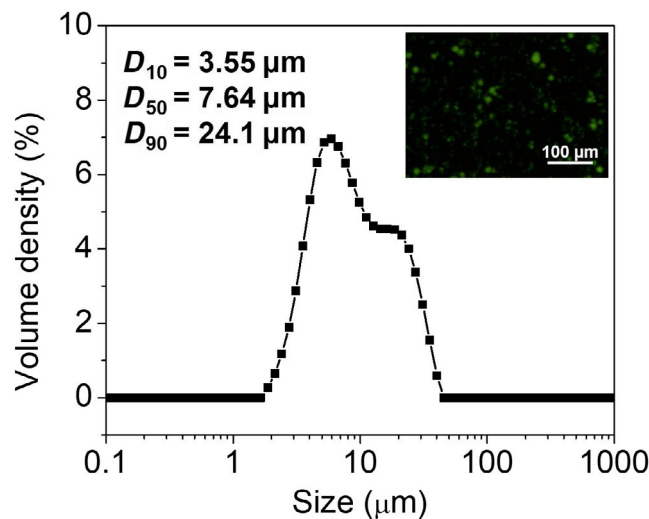


FIGURE 1 Particle size distribution of micro-gel particle suspension

suspension and HPAM solution were measured by Haake Mars III Rheometer (Thermo Scientific), as shown in Figure 3.

2.3 | Microchip design

The microchips used in this study were fabricated with the silicon material. The wettability is neutral for water (contact angle = $93.28 \pm 1.82^\circ$, Figure S1). After the design patterns were created, they were imported into AutoCAD using LISP (list procession language).³¹ The inlet and outlet ports and buffer regions, which located at the entrance and exit of the porous structures, were added in AutoCAD for introducing fluid into and out of the porous media region. The final porous structures were transferred to a silicon wafer using micro-fabrication techniques,^{34,37} including standard photolithography and inductively coupled plasma-deep reactive ion etching (ICP-DRIE). The prepared silicon wafer was bonded anodically to a Pyrex glass wafer (contact angle = $54.20 \pm 1.09^\circ$, Figure S2), the whole microchip in situ wettability was checked, and it was about neutral (Figure S3). The upstream and downstream of the Pyrex glass wafer were drilled with 2 mm diameter holes for the inlet and outlet of the microchip. The design of porous structures is very crucial for experiments, which will be introduced below in details.

2.3.1 | Bi-permeability micromodel design

The first goal of this work is to study the heterogeneity effect between reservoir layers. To purify this effect, we designed an artificial bi-permeability regular porous structure in micromodel as shown in Figure 4. The porous structure (8000 μ m length \times 6000 μ m width \times 60 μ m depth) contains

FIGURE 2 A, Cryo-SEM micrograph of micro-gel particle suspension and B, internal structure of the micro-gel particle, respectively

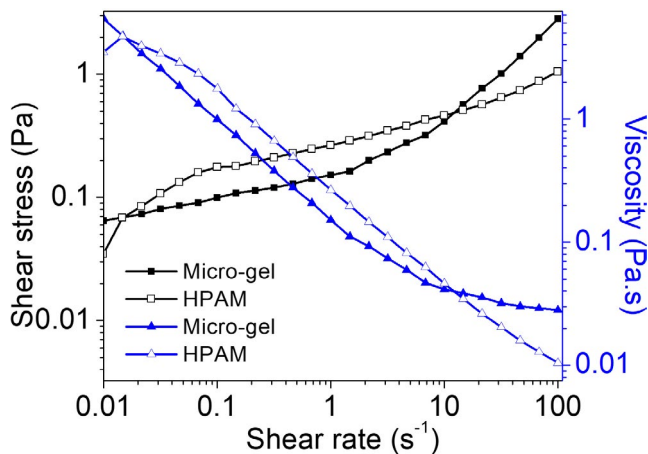
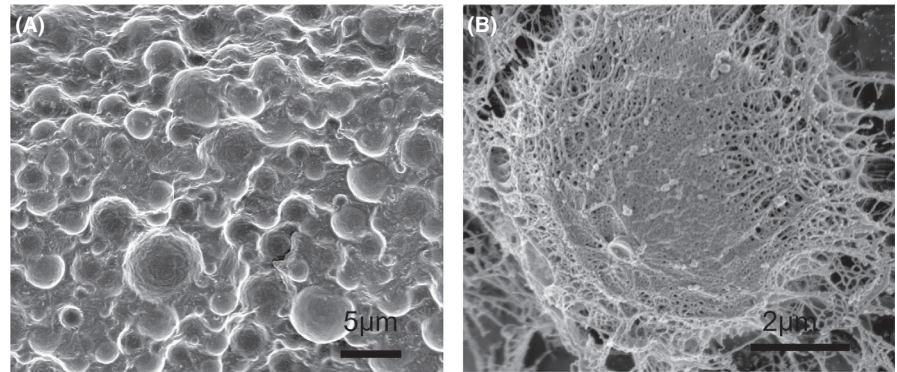


FIGURE 3 The shear stress and the apparent viscosity of micro-gel particle suspension and HPAM solution with the increase in shear rate

a high-permeable porous layer and a low-permeable porous layer, and the ends are connected to five equally distributed micro-channels (250 μm width for each), respectively. The high-permeable layer is composed of cylindrical pillars with a radius of 300 μm aligned at a distance of 120 μm , while the cylindrical pillars in the low-permeable layer have a radius of 150 μm aligned at a distance of 60 μm . The pore size is much larger than the micro-gel particle size. Both layers have the same porosity (45.45%), and the total volume is 1.31 μL . The permeability ratio of high-permeable layer and low-permeable layer was estimated at 16:9 with the hydraulic radii of the pore throats.³⁸ This simple design may help to better understand how the fluid channeling occurs and how to overcome it using the additives, such as polymer solutions or gel particles.

2.3.2 | Reservoir-on-a-chip design

The structured geometries in microfluidics work well for mechanism studies as they can purify the transport and interaction process. However, they still suffer much from industry society since the geometrical characteristics are far from the

real reservoirs, and therefore, the quantitative studies of EOR performance on microchips using structured geometries are not credible. For this reason, we propose a new strategy for reservoir-on-a-chip (ROC) design in this work. The concept of ROC was first proposed by Gunda et al³¹ to extend the traditional concept of lab-on-a-chip to reservoir engineering, and they used the pore-network model to abstract geometrical features of reservoir.

The crucial soul of ROC is to design appropriate porous structures that can reflect the most important information for transport of the concerned reservoir. For the (low-permeable) tight oil reservoirs in Changqing of China, we believe that two factors must be considered very carefully: the pore size distribution for microscale interaction of mechanics and the hierarchical pore structures for fluid flow in the unconventional reservoirs. Therefore, we propose a multi-step road map to design a porous structure on a ROC as illustrated in Figure 5.

First, microstructure characterization of cores from the concerned reservoir: Numerous and sufficient cores, low-permeable or extra-low-permeable sandstones from Changqing oilfield in China, were scanned by SEM, micro-CT, nano-CT, or FIB-SEM. Please note that the resolution of scanning should be higher than the critical resolution and the critical sample size need to satisfy the representative element volume (REV) condition rigidly during scanning.³⁹

Second, statistical information abstraction: After the pore structures reconstructed from the scanning data, by the image analysis software Fiji⁴⁰ in our work, the statistical information of reservoir geometries was abstracted, including pore distribution, connectivity, porosity, and so on. Based on our previous experience on multiphase displacement in rocks,⁴¹⁻⁴³ we believe that the pore size plays a key role on the oil development in tight reservoirs with micro/nano pores. The maximal ball algorithm^{44,45} was used to calculate the local pore size in the porous microstructures in this work.

Third, microstructure regeneration design for ROC: After the statistical information of reservoir geometries was abstracted from numerous samples, it was used for chip designs. We did not do mapping, yet we generated equivalent microstructures that could involve the most important and

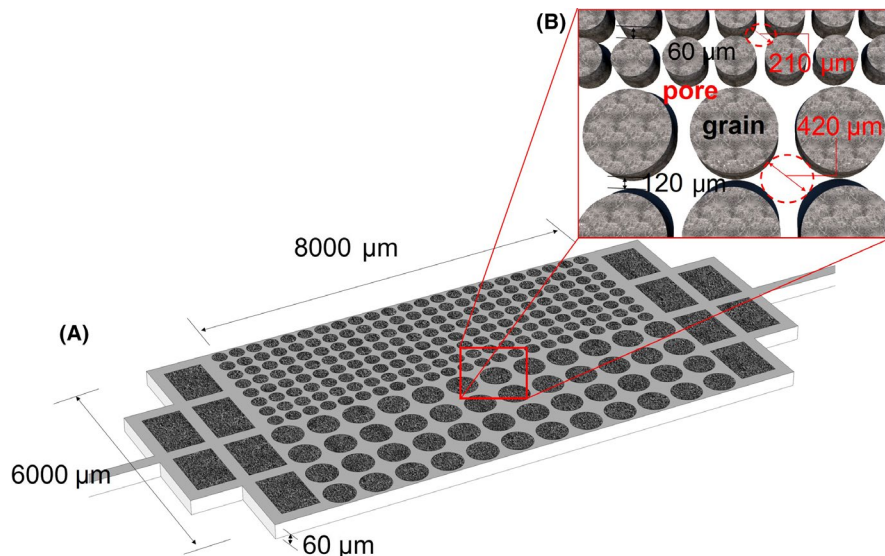


FIGURE 4 Schematic of the heterogeneous structured micromodel. A, Macroscopic image of the microchip; B, local image of grains and pores distribution

as much as possible statistical information of the real reservoir. To this effort, the QSGS algorithm^{35,36,46} was used to generate the geometry of the porous microstructures of ROC. As mentioned above, the two-dimensional porous structures on chips can never be the same as the three-dimensional ones of real rocks exactly, but the most important statistical information of geometries for transport and displacement process, such as the pore size distribution for tight reservoirs, has been embedded in the 2D designs for ROC.

Another important issue for chip design is on the hierarchical/multiscale pores/grains. Figure 6 illustrates that pores between large grains were filled with small grains to form small pores. Considering the formation features of pores in the reservoir rock specimen, two-step generation method based on QSGS was used in our work. In the first step, the large-size grains were either generated by QSGS or extracted from the large grain geometry database which was obtained from the CT-scanned image. The large grains, with the same number density as the real rock, were placed in the goal region stochastically of the microchip space. In the second step, the small-size grains were generated by QSGS in the remaining area until the goal pore size distribution was reached. Check the final pore size distribution of the geometry generated by QSGS until the geometry features get close enough to the ones of real reservoir rock.

After these characterization-statistics-regeneration steps, the reservoir-on-a-chip design is finally finished. One example based on the low-permeable tight sandstone oil reservoir in Changqing of China is shown in Figure 7. The mean pore size and the depth of the chip is designed as 39.5 μm , and the pore number is larger than 2.8×10^5 . The total pore volume of the chip V is 0.84 μL , and the porosity ρ is 44.39%. The hierarchical characteristics can be clearly seen in the right subfigure in Figure 7. The design embedded the most important statistical information

of target reservoir and can be used to study the micro-gel particle-based EOR mechanism in this reservoir. The next fabrication procession of ROC and bi-permeability microchip is the same as shown in Section 2.3.

2.4 | Experimental setup and procedure

The experimental setup of our microfluidic experiments is shown in Figure 8. The microchip is placed under an optical microscope (Nikon SMZ18) with a fluorescence module (excitation filter with bandpass wavelength $\lambda_{\text{ex}} = 460\text{-}500$ nm and receiving filter with bandpass wavelength $\lambda_{\text{em}} = 510$ nm), and the system is fitted with the Nile red dissolved in decane, whose fluorescent peak excitation wavelengths $\lambda_{\text{ex}} = 493$ nm and emission wavelengths $\lambda_{\text{em}} = 510$ nm.⁴⁷ The resolution of the microchip imaging was set as 1.92 μm per pixel to achieve micron-scale to centimeter-scale image. The flow inlet was connected to the stiffness syringe (Hamilton), which was mounted on the syringe pump (Longer) that allowed precise control of the injection flow rate. The experiments were conducted in normal temperature and pressure, regardless of the influence of temperature and salinity in the formation, and $Q = 1$ $\mu\text{L}/\text{min}$ was chosen as the fluid injection flow rate for the water, HPAM, and micro-gel particle suspension flooding. The macroscopic capillary number^{48,49} $Ca = \mu_{\text{oil}} v_{\text{in}} / \gamma$ is 1.75×10^{-6} (Bi-permeability) and 2.73×10^{-6} (ROC), where $\gamma = 46.60 \pm 0.25$ mN/m is the interfacial tension between water and decane, the characteristic injection velocity $v_{\text{in}} = QL/V$ is 1.02×10^{-4} m/s (Bi-permeability) and 1.59×10^{-4} m/s (ROC).

The pore space in the entire system needs to be saturated with oil before each displacing experiment. The microchip was cleaned by 50 pore volumes (PV) of cleaning solution (DI water: NH_4OH : H_2O_2 (volume ratio) = 5:1:1) and 50 PV of DI water sequentially. Then, the microchip

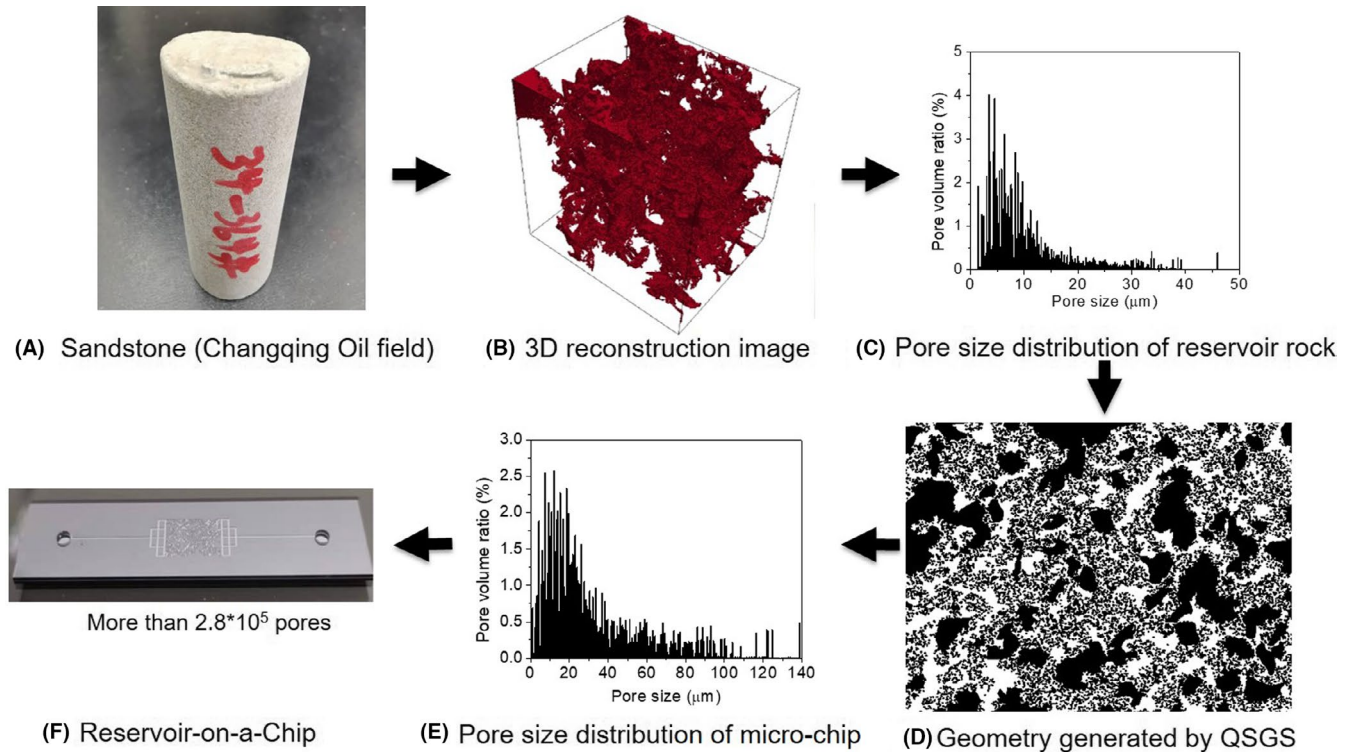
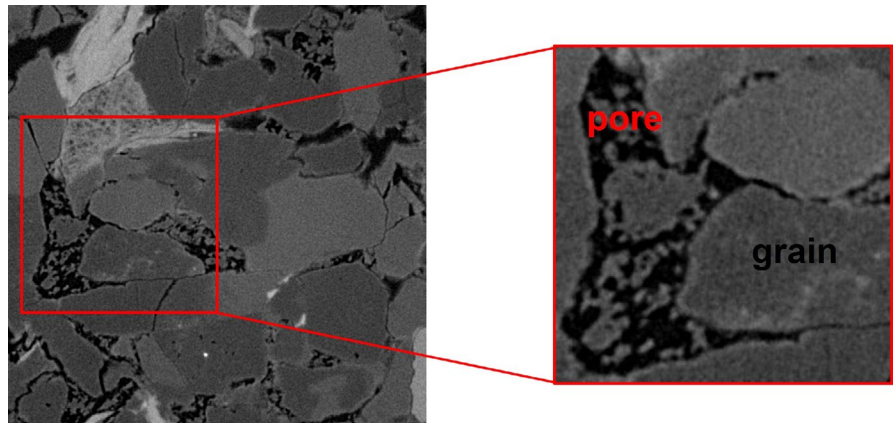


FIGURE 5 The flow map of reservoir-on-a-chip design

FIGURE 6 Micro-CT images to show the formation of the pores by different size grains. Dark represents pores and other colors are rock grains



was flooded with N_2 (1 bar) to dry the microchip and the vacuum treated for 12 hours. Finally, the fluorescent dyed oil was injected into the microchip with a relatively large flow rate (about $100 \mu\text{L}/\text{min}$ for 5 minutes) until all the pores were filled with oil. When the pressure difference is stable between the inlet and outlet, the switch changes to DI water, HPAM solution or micro-gel particle suspension syringe to start the displacing experiments. After the experiments, the Fiji software⁴⁰ was used for segmentation and processing of the images. Image stacks were converted to 8-bit and thresholded to binary pictures using the Otsu method.⁵⁰ Finally, the volume of oil and other fluids in the displacing procession was calculated.

3 | RESULTS AND DISCUSSION

3.1 | Bi-permeability micromodel experiments: transport mechanisms

Water flooding, HPAM solution flooding, and micro-gel particle suspension flooding experiments were conducted on the bi-permeability micromodel, respectively. Some important snapshots of water flooding, HPAM solution flooding, and micro-gel particle suspension flooding are compared in Figure 9, and the developments of displacement frontiers for high-permeable layer and low-permeable layer are shown in Figure 10.

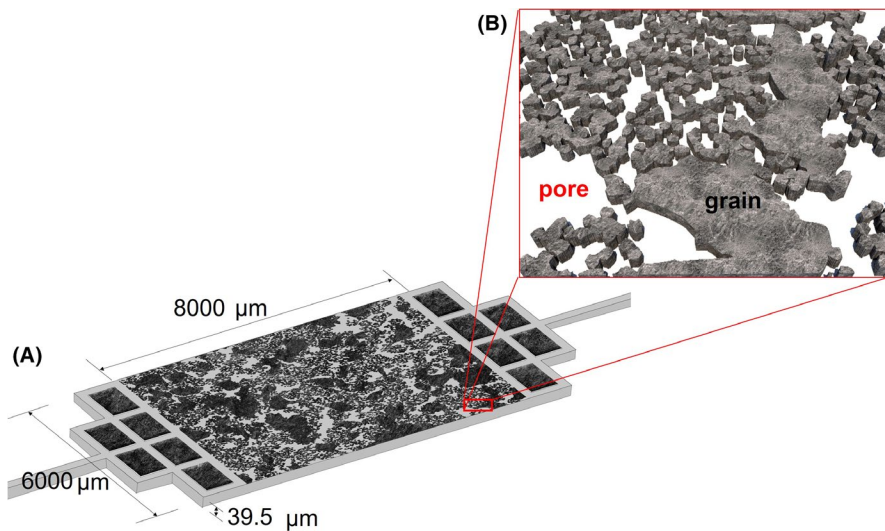


FIGURE 7 Schematic of Reservoir-on-a-Chip design. A, Overall image of the microchip; B, local image of grains and pores distribution. The mean pore size was $39.5 \mu\text{m}$, and pore number was larger than 2.8×10^5

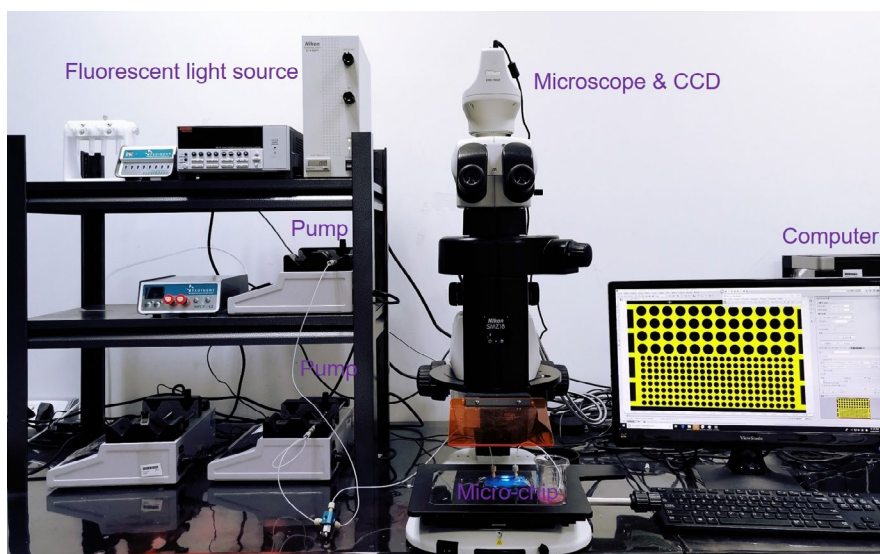


FIGURE 8 Image of the overall experimental setup

Fluid channeling was clearly shown in the water flooding experiment, shown in Figure 9(A). Water breaks through the high-permeable layer very fast and displacement frontier of low-permeable layer stops very early. Meanwhile, the water displacement frontier development curves for high-permeable layer and low-permeable layer are significantly different as shown in Figure 10 (see the black solid lines and open symbols). However, the HPAM solution and the micro-gel particle suspension, with the similar macroscopic rheology property (as shown in Figure 3), can overcome the fluid channeling phenomena well. But, the displacement performances are different, as shown in Figure 9(B,C). The flow field fluctuation is strong in micro-gel particle suspension flooding which may even cause the alternate displacement process, as shown in Figure 10 (see the red solid lines and solid symbols), while the HPAM solution flooding is quite stable, as shown in Figure 10 (see the blue dash lines and open symbols).

In order to show how the flow/pressure fluctuations are generated and developed, micro-gel particle suspension flooding was conducted in the same condition at the microscopic view, and the fluorescent micro-gel particles could be identified so that a local view of fluctuation phenomena may help to understand the micro-gel particle suspension flooding experiments, as shown in Figure 11. At the beginning, the micro-gel particle suspension would go into the high-permeable layer because of its smaller flow resistance. When the suspension flowed in the porous layer, it was observed that the gel particles lagged behind the water because of viscous dissipation. The result was that the particle concentration became lower at the position closer to the displacement frontier, and the suspension fluid in the high-permeable layer became denser and denser. Since the viscosity of micro-gel suspension increases dramatically with the particle concentration, as shown in Figure 12, the resistance of the high-permeable layer increase consequently. When the resistance

FIGURE 9 Snapshots of water flooding (A), HPAM solution flooding (B) and micro-gel particle suspension flooding (C), at 60, 120, 180, 220 s. The flow direction is from left to right. The scale bar represents 1000 μm . The blue phase is water, the cyan phase is HPAM solution, and green phase is micro-gel particle suspension

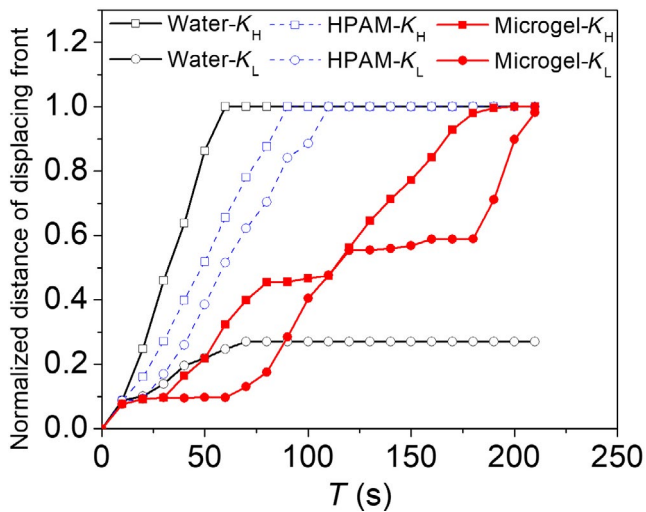
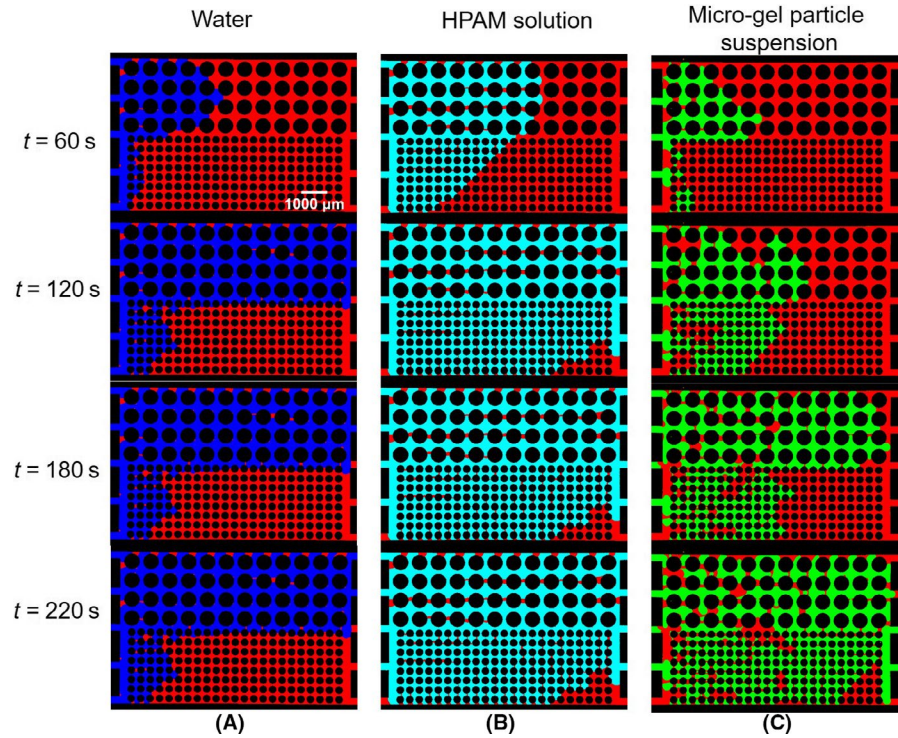


FIGURE 10 Displacement frontier development of water flooding experiments (black solid line and open symbols), HPAM solution flooding experiments (blue dash line and open symbols) and micro-gel particle suspension flooding experiments (red solid line and solid symbols) in high-permeable (square symbols) and low-permeable layer (circle symbols) region. K_H and K_L represent high-permeable layer and low-permeable layer separately

of the high-permeable layer reaches to higher than that of the low-permeable layer, the flow priority switches to the low-permeable layer so that the oil in the low-permeable layer will be displaced. The flow path may switch more when the resistance contrast changes between high- and low-permeable layers, which results in the flow or pressure fluctuation to enhance the oil recovery.

In the bi-permeability micromodel experiments, the high-permeable layer and the low-permeable layer are parallel. The pressure drops of the high-permeable and low-permeable layer have the same value. Darcy's law of high-permeable layer in Equation (1) and low-permeable layer in Equation (2) can be combined. The displacement frontier velocity ratio (u_{f_H}/u_{f_L}) can be determined by the mobility ratio $((\mu_{f_L} k_{r_H})/(\mu_{f_H} k_{r_L}))$ of the displacing fluid in high-permeable layer and low-permeable layer, shown in Equation (3).

$$u_{f_H} = -\frac{k_H k_{r_H} \nabla P}{\mu_{f_H}} \quad (1)$$

$$u_{f_L} = -\frac{k_L k_{r_L} \nabla P}{\mu_{f_L}} \quad (2)$$

$$\frac{u_{f_H}}{u_{f_L}} = \frac{k_H k_{r_H} \mu_{f_L}}{k_L k_{r_L} \mu_{f_H}} = \frac{16}{9} \frac{\mu_{f_L}/k_{r_L}}{\mu_{f_H}/k_{r_H}} \quad (3)$$

where the subscript H and L represent the high-permeable layer and the low-permeable layer, respectively. The u_{f_H} and u_{f_L} are velocities of displacing fluid in high-permeable layer and low-permeable layer, respectively. The k_H/k_L is the intrinsic permeability ratio. μ_f is displacing fluid viscosity, and k_r is relative permeability of displacing fluid phase.

As the two-phase Darcy's law is phenomenological, the precise dependencies for key parameters, for example, k_r , have no clear physical meaning. k_r can be determined on

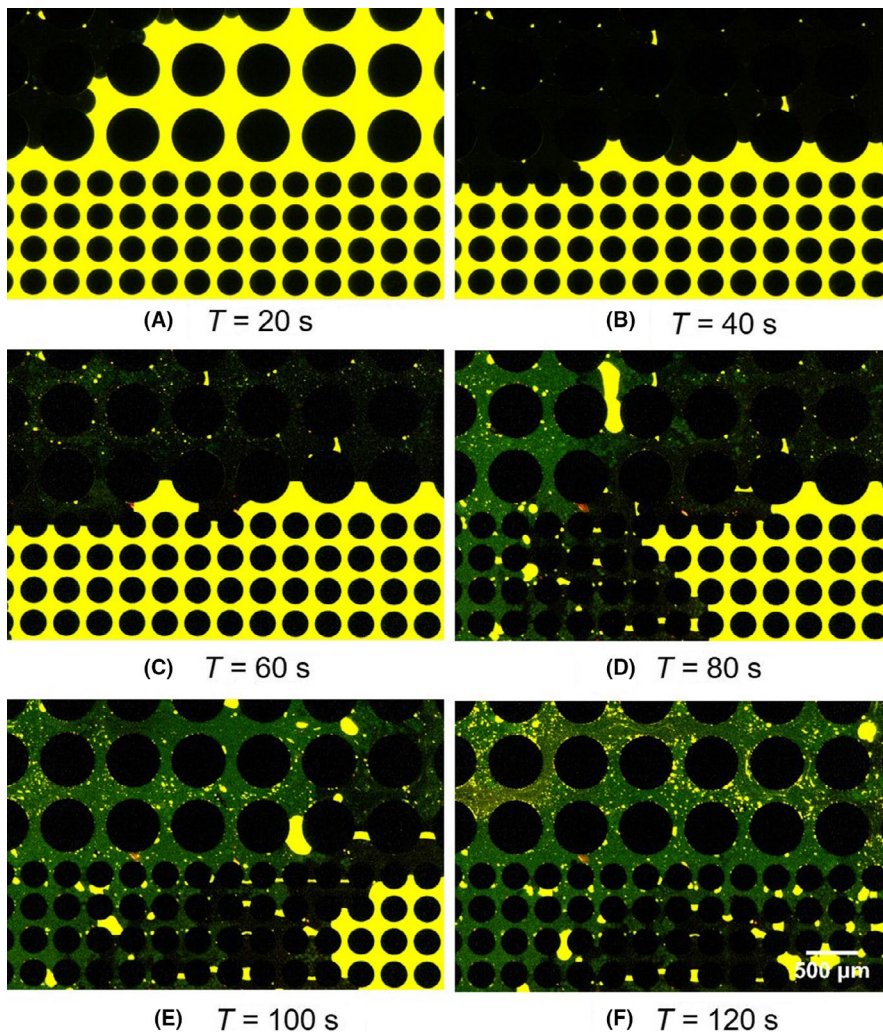


FIGURE 11 Original microscopic image of local fluctuation phenomena during injection of micro-gel particle suspension, at 20, 40, 60, 80, 100, 120 s, respectively. The flow direction of each picture is from left to right. The scale bar represents 500 μm . The dark phase is water, the green phase is micro-gel particle suspension, and yellow phase is oil

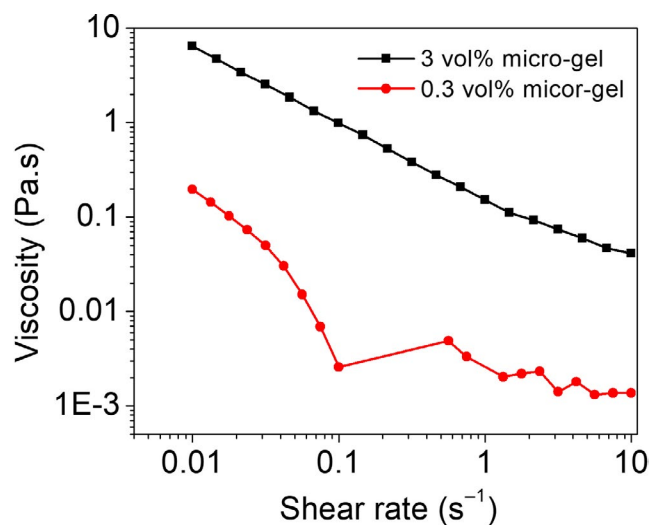


FIGURE 12 The viscosity of the micro-gel particle suspension is very sensitive to the changes in its concentration. The highly concentrated micro-gel particle suspension (original suspension) was diluted to 3 vol% (black line and solid squares) and 0.3 vol% (red line and solid circles) by DI water, and they were measured by Haake Mars III Rheometer (Thermo Scientific)

system history and flow rate for the same pair of fluids and porous media.⁵¹ In our study, the similar rheology properties of displacing fluid and the same porous structure were used on the same experimental conditions, and we thought that the relative permeability should obey the same curve between HPAM solution and micro-gel particle suspension. For the HPAM flooding experiments, the concentration of the HPAM was constant, so that the displacing front velocity ratio (u_{f_H}/u_{f_L}) could be determined by the relative permeability ratio (k_{r_H}/k_{r_L}), which could not cause the fluid field fluctuation in the HPAM solution flooding. However, the nonuniform concentration of micro-gel particle in suspension was observed in the experiments, as shown in Figures 11 and 12. Lower concentration of micro-gel particle suspension leads to lower viscosity, for example, dilution 10 times of micro-gel particle suspension concentration results in a nearly 100-fold decrease in viscosity. Therefore, the concentration of micro-gel particle suspension influences fluid mobility in high-permeable layer and low-permeable layer. Nonuniform micro-gel particle concentration distribution in heterogeneous porous media will cause the mobility contrast in different

permeable layer changing frequently and induced the fluid field fluctuation finally.

3.2 | Reservoir-on-a-chip experiments: EOR performances

The micromodel experiments on bi-permeability-layer chip clearly show that the flow field fluctuation may be strong in micro-gel particle suspension flooding due to the nonuniform concentration distribution of micro-gel particles. However, such structured geometries are far from the complex geometries in real rocks and hard to evaluate the EOR performances. Therefore, experiments based on reservoir-on-a-chip have been conducted to quantify this effect for EOR.

By visualizing the two-phase distribution, the snapshots in both the global view and the local view are shown in Figure 13 for HPAM flooding and micro-gel suspension flooding. At the beginning stage (0.157-1.57 PV), some clustered oil is trapped by both HPAM solution and micro-gel suspension flooding. As the flooding going on, the clustered oil becomes stable and hardly recovered for a long time by the HPAM solution flooding, but still can be sliced and recovered by the micro-gel particle suspension flooding continuously. In the micro-gel suspension flooding, the fluctuation effect is strong in the swept residual oil area.

3.2.1 | Displacement efficiency & sweep efficiency

Two important performance parameters are used to evaluate EOR methods: one is the sweep efficiency, and the other is the micro-displacement efficiency.⁵² The total oil recovery E_R can be calculated by Equation (4). The sweep efficiency E_v is defined as Equation (5), with the ratio of swept pore volume V_{sw} and total pore volume V_{total} . The micro-displacement efficiency E_m is defined as Equation (6), with the ratio of recovered oil saturation in the swept volume S_o-S_{or} and swept volume oil saturation S_o .

$$E_R = E_v E_m \quad (4)$$

$$E_v = V_{sw} / V_{total} \quad (5)$$

$$E_m = (S_o - S_{or}) / S_o \quad (6)$$

In order to calculate the displacement efficiency and the sweep efficiency, the residual oil is classified in this work into two types: (a) nonswept oil defined as the residual oil with the volume larger than 1% PV, and (b) residual oil in the swept region defined as the residual oil with the volume <1% PV. The decomposition process of the residual oil image is demonstrated in Figure 14.

The sweep efficiency and the displacement efficiency curves of HPAM solution flooding and micro-gel particle

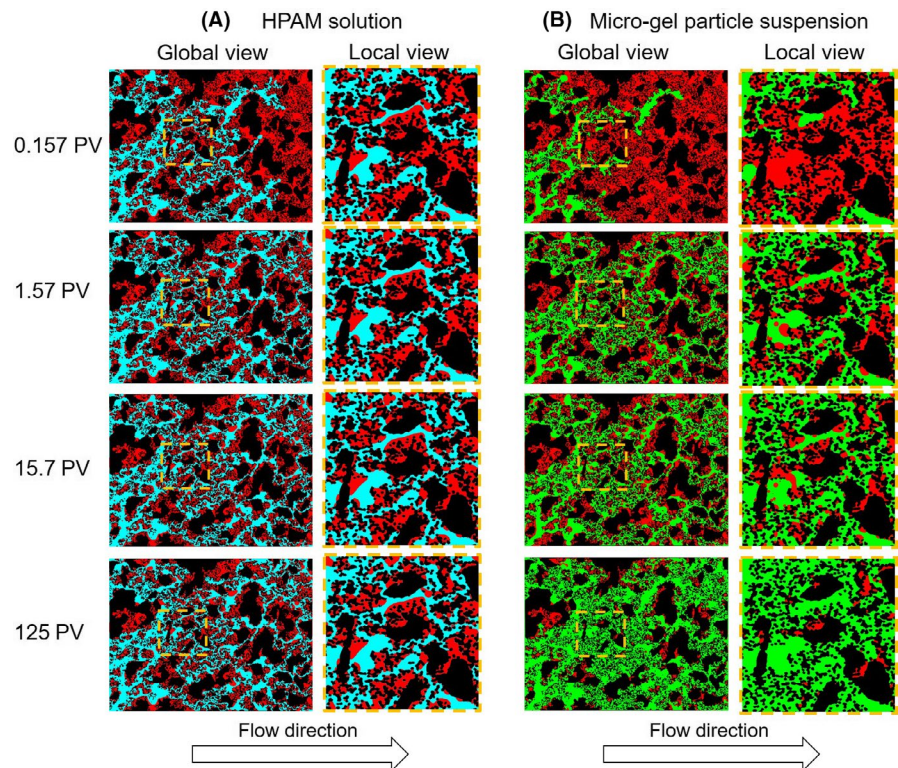


FIGURE 13 The snapshots in the global view and the local view of reservoir-on-a-chip experiments at 0.157 PV, 1.57 PV, 15.7 PV, and 125 PV. A, HPAM solution flooding experiment. HPAM solution: cyan, oil: red; B, micro-gel particle suspension flooding experiment. Micro-gel particle suspension: green, oil: red. The flow direction of each picture is from left to right. Global view shows the porous media region (6×8 mm) of ROC, local view region is selected randomly from the porous media (2×2 mm)

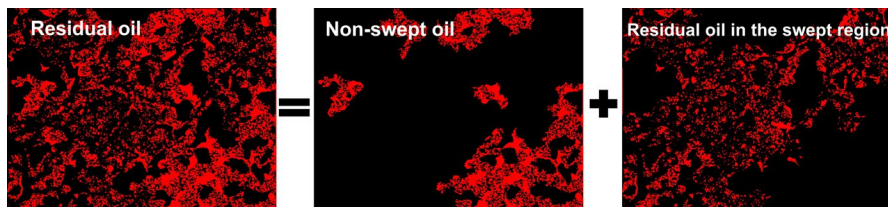


FIGURE 14 The schematic picture of separating residual oil as nonswept oil and residual oil in the swept region

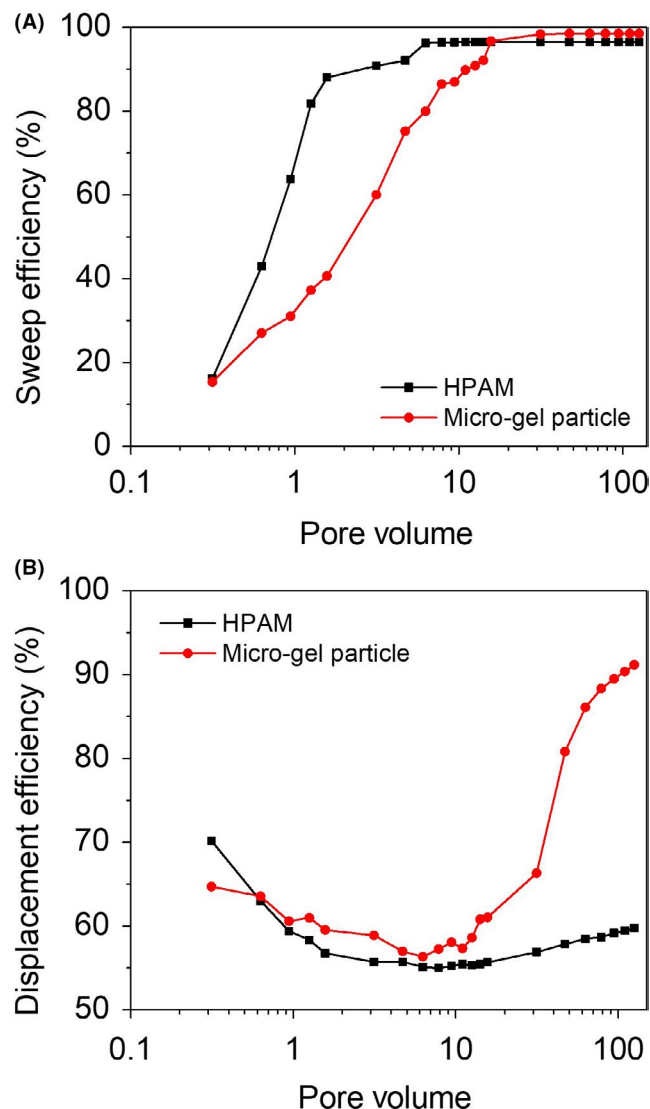


FIGURE 15 A, Sweep efficiency and B, displacement efficiency curves by the reservoir-on-a-chip experiments

suspension flooding are compared in Figure 15. At the beginning stage (0-1.57 PV), the HPAM solution can sweep the relative larger area, as shown in Figure 15(A), but the micro-gel particle suspension can reach the same level after a while (>15.7 PV). This result is consistent with the pictures in Figure 13. The displacement efficiency of micro-gel suspension flooding increases fast after 15.7 PV injection, as shown in Figure 15(B), which means that the clustered oil trapped in swept region is recovered, as shown in Figure 13.

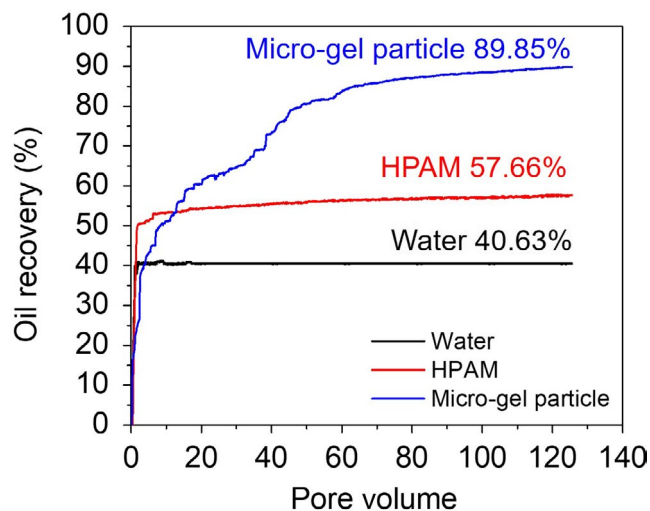


FIGURE 16 Oil recovery curve during the reservoir-on-a-chip experiments

3.2.2 | Oil recovery curve

The recovery rate is a very important parameter to evaluate the performance of recovery methods. Figure 16 compares the recovery curves of the three concerned methods by our ROC experiments. The water flooding reached a 40.63% oil recovery on the chip reservoir. The HPAM flooding increased the oil recovery significantly, and 57.66% oil can be recovered. The recovery curve of HPAM flooding was similar with the water flooding, which rose quickly at the beginning stage and got stable very soon. It was surprising to find that the micro-gel particle suspension flooding raised the recovery rate up to 89.85%. Even though the displacing performance of micro-gel suspension flooding was lower than the other two methods at the beginning stage, its EOR performance lasted for a long time. This means that the flow/pressure field fluctuation in the micro-gel particle suspension flooding may displace more oil out, which is not able to be recovered by other methods, and improve the displacement efficiency continuously.

4 | CONCLUSIONS

This paper presents a strategy to design microchips with the most important statistical information of concerned reservoir geometries. Taking the tight sandstone reservoir in Changqing of China as an example, we demonstrate the multi-step road

map for reservoir-on-a-chip designs. Especially for such a low-permeable sandstone reservoir, the pore size distribution and hierarchical grain size feature play the key roles on microscale transport and displacement interactions, and they were embedded seriously in the designs. On the microfluidic visualization platform, flooding experiments have been conducted on structured micromodel for EOR mechanism study or on reservoir-on-a-chip for EOR performance evaluation, using micro-gel particle suspension compared with water and polymer solution. Based on measurements and analysis, we draw the following conclusions:

- The flooding experiments on bi-permeability micromodels show that both micro-gel particle suspension and HPAM solution can overcome the fluid channeling and displace the oil in the low-permeable layer out. Different with the viscous effect of HPAM solution, the EOR mechanism of micro-gel suspension is caused by flow priority switch between low- and high-permeability layers, which can be ascribed to the particle concentration automatic redistribution during flow in porous structures. The switch does not only cause the alternate displacement process but also induce strong fluid field fluctuation.
- The flooding experiments on ROC with hierarchical porous structures show that the clustered oil trapped in the swept pores can hardly be moved by water and HPAM solution, but can be recovered by micro-gel particle suspension gradually due mainly to the fluid field fluctuation, which actually increases the displacement efficiency for a long time and enhances the oil recovery significantly.
- The flooding experiments on ROC make it possible to quantify the oil recovery rate for the concerned reservoir in laboratory. The recovery curves show that both the water flooding and the HPAM flooding recoveries rise quickly at the beginning stage and get stable very soon, while the micro-gel particle suspension flooding recovers oil slower than the other two methods but gets the best recovery finally. The water flooding reached a stable 40.63% oil recovery on the chip reservoir. The HPAM flooding increased the oil recovery significantly and 57.66% oil can be recovered. The micro-gel particle suspension flooding raised the recovery rate surprisingly up to 89.85% on the chip. These results indicate that micro-gel particle suspension flooding is very promising for EOR in industrial applications.

ACKNOWLEDGMENTS

This work is financially supported by the NSF grant of China (Nos. U1837602, 91634107) and the National Science and Technology Major Project on Oil and Gas (No. 2017ZX05013001). We would like to sincerely thank Dr Ke Xu from Massachusetts Institute of Technology for some suggestions in building up microfluidics experimental setup and Dr Mengquan Shi from Technical Institute of Physics

and Chemistry, Chinese Academy of Sciences for providing the micro-gel particles with fluorescence.

ORCID

Moran Wang  <https://orcid.org/0000-0002-0112-5150>

REFERENCES

1. Chu S, Majumdar A. Opportunities and challenges for a sustainable energy future. *Nature*. 2012;488(7411):294.
2. Al Adasani A, Bai B. Analysis of EOR projects and updated screening criteria. *J Petrol Sci Eng*. 2011;79(1–2):10–24.
3. Kamal MS, Sultan AS, Al-Mubaiyeh UA, Hussein IA. Review on polymer flooding: rheology, adsorption, stability, and field applications of various polymer systems. *Polym Rev*. 2015;55(3):491–530.
4. Imqam A, Bai B. Optimizing the strength and size of preformed particle gels for better conformance control treatment. *Fuel*. 2015;148:178–185.
5. Han D, Yang C, Zhang Z, Lou Z, Chang Y. Recent development of enhanced oil recovery in China. *J Petrol Sci Eng*. 1999;22(1):181–188.
6. Wever DAZ, Picchioni F, Broekhuis AA. Polymers for enhanced oil recovery: a paradigm for structure–property relationship in aqueous solution. *Prog Polym Sci*. 2011;36(11):1558–1628.
7. Xia H, Wang D, Wang G, Ma W-G, Deng HW, Liu J. Mechanism of the effect of micro-forces on residual oil in chemical flooding. *SPE symposium on improved oil recovery*. Tulsa, Oklahoma, USA: Society of Petroleum Engineers; 2008.
8. Farajzadeh R, Andrianov A, Krastev R, Hirasaki GJ, Rossen WR. Foam–oil interaction in porous media: implications for foam assisted enhanced oil recovery. *Adv Coll Interface Sci*. 2012;183–184:1–13.
9. Ma K, Lontas R, Conn CA, Hirasaki GJ, Biswal SL. Visualization of improved sweep with foam in heterogeneous porous media using microfluidics. *Soft Matter*. 2012;8(41):10669.
10. Jia B, Tsau J-S, Barati R. A review of the current progress of CO₂ injection EOR and carbon storage in shale oil reservoirs. *Fuel*. 2019;236:404–427.
11. Bai B, Liu Y, Coste J-P, Li L. Preformed particle gel for conformance control: transport mechanism through porous media. *SPE Reservoir Eval Eng*. 2007;10(02):176–184.
12. Ranganathan R, Lewis R, McCool CS, Green DW, Willhite GP. Experimental study of the gelation behavior of a polyacrylamide/aluminum citrate colloidal-dispersion gel system. *SPE J*. 1998;3(04):337–343.
13. Zhao G, You Q, Tao J, et al. Preparation and application of a novel phenolic resin dispersed particle gel for in-depth profile control in low permeability reservoirs. *J Petrol Sci Eng*. 2018;161:703–714.
14. Yang H, Kang W, Wu H, et al. Stability, rheological property and oil-displacement mechanism of a dispersed low-elastic microsphere system for enhanced oil recovery. *RSC Adv*. 2017;7(14):8118–8130.
15. Yao C, Lei G, Cathles LM, Steenhuis TS. Pore-scale investigation of micron-size polyacrylamide elastic microspheres (MPeMs) transport and retention in saturated porous media. *Environ Sci Technol*. 2014;48(9):5329–5335.
16. Dickinson E. Structure and rheology of colloidal particle gels: insight from computer simulation. *Adv Coll Interf Sci*. 2013;199:114–127.
17. Lei W, Xie C, Wu T, Wu X, Wang M. Transport mechanism of deformable micro-gel particle through micropores with mechanical properties characterized by AFM. *Sci Rep*. 2019;9(1):1453.

18. Li J, Jiang Z, Wang Y, Zheng J, Huang G. Stability, seepage and displacement characteristics of heterogeneous branched-preformed particle gels for enhanced oil recovery. *RSC Adv.* 2018;8(9):4881-4889.
19. Pritchett J, Frampton H, Brinkman J, et al. Application of a new in-depth waterflood conformance improvement tool. *SPE international improved oil recovery conference in Asia Pacific.* Kuala Lumpur, Malaysia: Society of Petroleum Engineers; 2003.
20. Almohsin AM, Bai B, Imqam AH, et al. Transport of nanogel through porous media and its resistance to water flow. *SPE improved oil recovery symposium.* Tulsa, Oklahoma, USA: Society of Petroleum Engineers; 2014.
21. Smith JE, Liu H, Guo Z. Laboratory studies of in-depth colloidal dispersion gel technology for Daqing oil field. *SPE/AAPG western regional meeting.* Long Beach, California: Society of Petroleum Engineers. 2000:13.
22. Imqam A, Bai B, Delshad M. Micro-particle gel transport performance through unconsolidated sandstone and its blocking to water flow during conformance control treatments. *Fuel.* 2018;231:479-488.
23. Sinton D. Energy: the microfluidic frontier. *Lab Chip.* 2014;14(17):3127-3134.
24. Lifton VA. Microfluidics: an enabling screening technology for enhanced oil recovery (EOR). *Lab Chip.* 2016;16(10):1777-1796.
25. O'Connell MG, Lu NB, Browne CA, Datta SS. Cooperative size sorting of deformable particles in porous media. *Soft Matter.* 2019;15(17):3620-3626.
26. Anbari A, Chien HT, Datta SS, Deng W, Weitz DA, Fan J. Microfluidic model porous media: fabrication and applications. *Small.* 2018;14(18):1703575.
27. Chen Y, Li Y, Valocchi AJ, Christensen KT. Lattice Boltzmann simulations of liquid CO₂ displacing water in a 2D heterogeneous micromodel at reservoir pressure conditions. *J Contam Hydrol.* 2018;212:14-27.
28. Clemens T, Tsikouris K, Buchgraber M, Castanier LM, Kovscek A. Pore-scale evaluation of polymers displacing viscous oil - computational-fluid-dynamics simulation of micromodel experiments. *SPE Reservoir Eval Eng.* 2013;16(2):144-154.
29. Yamada M, Seki M. Hydrodynamic filtration for on-chip particle concentration and classification utilizing microfluidics. *Lab Chip.* 2005;5(11):1233-1239.
30. Lenormand R, Zarccone C, Sarr A. Mechanisms of the displacement of one fluid by another in a network of capillary ducts. *J Fluid Mech.* 1983;135(135):337-353.
31. Kumar Gunda NS, Bera B, Karadimitriou NK, Mitra SK, Hassanizadeh SM. Reservoir-on-a-chip (ROC): a new paradigm in reservoir engineering. *Lab Chip.* 2011;11(22):3785-3792.
32. Xu K, Agrawal D, Darugar Q. Hydrophilic nanoparticle-based enhanced oil recovery: microfluidic investigations on mechanisms. *Energy Fuels.* 2018;32(11):11243-11252.
33. Mejia L, Tagavifar M, Xu K, Mejia M, Du Y, Balhoff M. Surfactant flooding in oil-wet micromodels with high permeability fractures. *Fuel.* 2019;241:1117-1128.
34. Zuo L, Zhang C, Falta RW, Benson SM. Micromodel investigations of CO₂ exsolution from carbonated water in sedimentary rocks. *Adv Water Resour.* 2013;53:188-197.
35. Wang M, Wang J, Pan N, Chen S. Mesoscopic predictions of the effective thermal conductivity for microscale random porous media. *Phys Rev E.* 2007;75(3):036702.
36. Wang M, Pan N. Predictions of effective physical properties of complex multiphase materials. *Mater Sci Eng: R: Rep.* 2008;63(1):1-30.
37. Chomsurin C, Werth CJ. Analysis of pore-scale nonaqueous phase liquid dissolution in etched silicon pore networks. *Water Resour Res.* 2003;39(9):1265.
38. Carman PC. Fluid flow through granular beds. *Chem Eng Res Des.* 1997;75:S32-S48.
39. Liu T, Jin X, Wang M. Critical resolution and sample size of digital rock analysis for unconventional reservoirs. *Energies.* 2018;11(7):1798.
40. Schindelin J, Arganda-Carreras I, Frise E, et al. Fiji: an open-source platform for biological-image analysis. *Nat Methods.* 2012;9:676.
41. Xie C, Raeini AQ, Wang Y, Blunt MJ, Wang M. An improved pore-network model including viscous coupling effects using direct simulation by the lattice Boltzmann method. *Adv Water Resour.* 2017;100:26-34.
42. Zheng J, Ju Y, Wang M. Pore-scale modeling of spontaneous imbibition behavior in a complex shale porous structure by pseudo-potential lattice Boltzmann method. *J Geophys Res-Solid Earth.* 2018;123(11):9586-9600.
43. Xie C, Lv W, Wang M. Shear-thinning or shear-thickening fluid for better EOR?—a direct pore-scale study. *J Petrol Sci Eng.* 2018;161:683-691.
44. Al-Kharusi AS, Blunt MJ. Network extraction from sandstone and carbonate pore space images. *J Petrol Sci Eng.* 2007;56(4):219-231.
45. Guo Y, He X, Huang W, Wang M. Microstructure effects on effective gas diffusion coefficient of nanoporous materials. *Transp Porous Media.* 2019;126(2):431-453.
46. Zhang L, Wang M. Modeling of electrokinetic reactive transport in micropore using a coupled lattice Boltzmann method. *J Geophys Res: Solid Earth.* 2015;120(5):2877-2890.
47. Grate JW, Zhang C, Wietsma TW, et al. A note on the visualization of wetting film structures and a nonwetting immiscible fluid in a pore network micromodel using a solvatochromic dye. *Water Resour Res.* 2010;46(11):W11602.
48. Lenormand R, Touboul E, Zarccone C. Numerical models and experiments on immiscible displacements in porous media. *J Fluid Mech.* 1988;189(189):165-187.
49. Zhao B, MacMinn CW, Juanes R. Wettability control on multiphase flow in patterned microfluidics. *Proc Natl Acad Sci USA.* 2016;113(37):10251-10256.
50. Otsu N. A threshold selection method from gray-level histograms. *IEEE Trans Syst Man Cybernetics.* 1979;9(1):62-66.
51. Armstrong RT, McClure JE, Berrill MA, Rücker M, Schlüter S, Berg S. Beyond Darcy's law: the role of phase topology and ganglion dynamics for two-fluid flow. *Phys Rev E.* 2016;94(4):043113.
52. Morrow NR. *Interfacial phenomena in petroleum recovery.* New York: Marcel Dekker; 1991.

SUPPORTING INFORMATION

Additional supporting information may be found online in the Supporting Information section.

How to cite this article: Lei W, Liu T, Xie C, Yang H, Wu T, Wang M. Enhanced oil recovery mechanism and recovery performance of micro-gel particle suspensions by microfluidic experiments. *Energy Sci Eng.* 2020;8:986–998. <https://doi.org/10.1002/ese3.563>